CANCER

Mechanical manipulation of cancer cell tumorigenicity via heat shock protein signaling

Siu Hong Dexter Wong[1,2,3]†, Bohan Yin[1,2]†, Zhuo Li[4], Weihao Yuan[4], Qin Zhang[2], Xian Xie[4], Youhua Tan[2,5], Nathalie Wong[6], Kunyu Zhang[7,8,9,10]*, Liming Bian[7,8,9,10]*

Biophysical cues of rigid tumor matrix play a critical role in cancer cell malignancy. We report that stiffly confined cancer cells exhibit robust growth of spheroids in the stiff hydrogel that exerts substantial confining stress on the cells. The stressed condition activated Hsp (heat shock protein)–signal transducer and activator of transcription 3 signaling via the transient receptor potential vanilloid 4–phosphatidylinositol 3-kinase/Akt axis, thereby up-regulating the expression of the stemness-related markers in cancer cells, whereas these signaling activities were suppressed in cancer cells cultured in softer hydrogels or stiff hydrogels with stress relief or Hsp70 knockdown/inhibition. This mechanopriming based on three-dimensional culture enhanced cancer cell tumorigenicity and metastasis in animal models upon transplantation, and pharmaceutically inhibiting Hsp70 improved the anticancer efficacy of chemotherapy. Mechanistically, our study reveals the crucial role of Hsp70 in regulating cancer cell malignancy under mechanically stressed conditions and its impacts on cancer prognosis–related molecular pathways for cancer treatments.

INTRODUCTION

Tumorigenesis is known to strongly depend on biophysical factors of the tumor microenvironment (TME), including extracellular matrix (ECM) stiffness (*1–4*). Deviation from mechanical homeostasis at the cell and tissue levels is associated with developmental abnormalities and cancer (*5*, *6*). Tumors are generally stiffer than normal tissues because of the increased cross-linking of tumor ECM (*7*, *8*). In addition, the proliferation of cancer cells results in the counteractive resistance of ECM to the expanding tumor volume generated by the deformed surrounding stromal tissue and high tumor stiffness, building up the intratumoral stress that can further promote tumor progression (*9*, *10*). However, the molecular mechanism by which mechanically stressed conditions in the three-dimensional (3D) TME promote tumorigenesis in cancer cells remains unclear.

Stress-inducible heat shock protein 70 (Hsp70) is a class of molecular chaperones required for cell survival by buffering proteotoxic insults, such as thermal and mechanical stress (*11–13*). Previous studies suggested that Hsp70 expression was elevated in vascular smooth muscle cells and intervertebral disc cells in response to mechanical stress (*11*, *14*). Another report indicated that a lack of Hsp70 in murine breast cancer cells leads to poor tumor initiation and metastasis in host mice (*15*). These findings indicate that Hsp70 may play a key role in regulating cancer cell tumorigenicity in response to mechanical stresses. However, to our knowledge, no previous studies have investigated the molecular mechanism of Hsp signaling activation in mechanoprimed cancer cells.

Hydrogel-based 3D culture systems are promising for building cancer spheroids that recapitulate the distinct physiological and pathological features of solid tumors in vitro. The cross-linked polymer network of hydrogels with tunable biophysical properties can be customized to recreate the biomimetic microenvironment (*16*, *17*). These systems enable the generation of tumor equivalents with defined biochemical and biophysical properties that can be instrumental in elucidating tumor pathogenesis. Nevertheless, fabricating hydrogels with tunable mechanical properties while controlling other consistent parameters is the key to decoupling the impact of mechanical cues imposed by the TME on cancer cell development.

Hyaluronic acid (HA) is one of the ubiquitous components of ECM with high stability against nonspecific enzymatic activities and is an ideal building block to fabricate hydrogels for a 3D culture of cancer cells (*18*). Here, we fabricated HA-based hydrogels with a wide range of stiffnesses (2 to 100 kPa) while keeping the biochemical content the same to examine the impact of matrix stiffness on cancer cell growth and tumorigenicity (Fig. 1A). Our findings showed that cancer cells in stiff hydrogels exhibited much more robust cell proliferation and developed into larger spheroidal colonies than those in softer hydrogels (Fig. 1, B and C). Stress relief of the stiff hydrogel via degradation-induced hydrogel softening caused the expansion of cancer spheroids and nuclear size expansion (Fig. 1, B and C), indicating high confining stress on cancer cells. This stress elevated the expression levels of Hsp70 via the transient receptor potential vanilloid 4 (TRPV4)–phosphatidylinositol 3-kinase (PI3K)/Akt–heat shock factor 1 (HSF1) signaling axis

¹School of Medicine and Pharmacy, Ocean University of China, Qingdao 266003, P. R. China. ²Department of Biomedical Engineering, The Hong Kong Polytechnic University, Hong Kong 999077, P. R. China. ³Research Institute for Sports Science and Technology, The Hong Kong Polytechnic University, Kowloon, Hong Kong 999077, P. R. China. ⁴Department of Biomedical Engineering, The Chinese University of Hong Kong, Hong Kong 999077, P. R. China. ⁵The Hong Kong Polytechnic University Shenzhen Research Institute, Shenzhen 518057, P. R. China. ⁶Department of Surgery, The Chinese University of Hong Kong, Hong Kong 999077, P. R. China. ⁷School of Biomedical Sciences and Engineering, Guangzhou International Campus, South China University of Technology, Guangzhou 511442, P. R. China. ⁸National Engineering Research Center for Tissue Restoration and Reconstruction, South China University of Technology, Guangzhou 510006, P. R. China. ⁹Guangdong Provincial Key Laboratory of Biomedical Engineering, South China University of Technology, Guangzhou 510006, P. R. China. ¹⁰Key Laboratory of Biomedical Materials and Engineering of the Ministry of Education, South China University of Technology, Guangzhou 510006, P. R. China.
*Corresponding author. Email: kyuzhang@scut.edu.cn (K.Z.); bianlm@scut.edu.cn (L.B.)
†These authors contributed equally to this work.
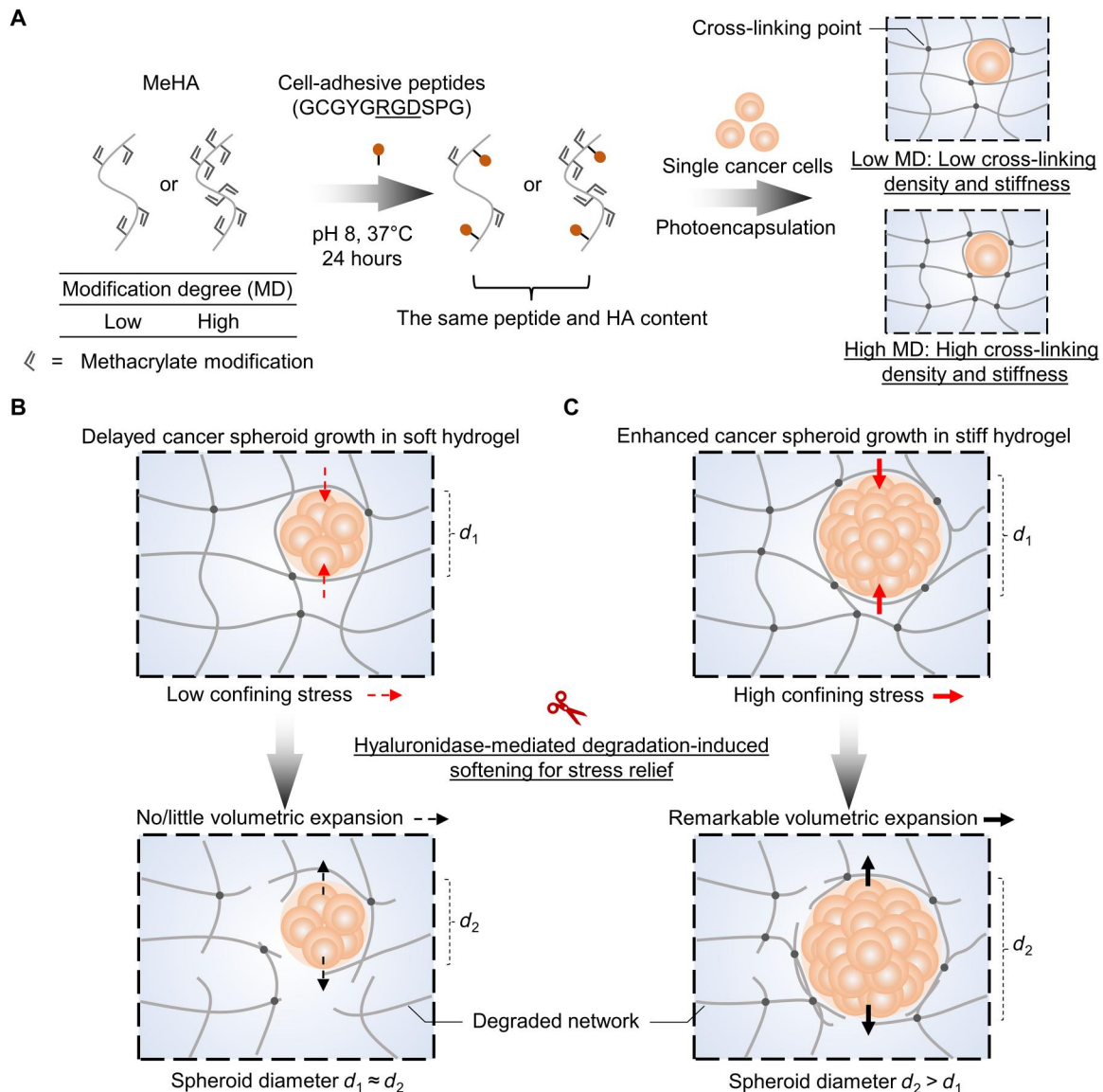
Fig. 1. Schematic illustration of the differential compressive confining stress imposed by hydrogels of varying rigidities on cancer cells and its impact on the growth of cancer spheroids in hydrogels. (**A**) Fabrication of methacrylated hyaluronic acid (MeHA) hydrogels with varying cross-linking densities by changing the modification degree (MD) while controlling the HA content. Single cancer cells were dispersed in precursor solutions of MeHA with varying MDs that were coupled to the same amount of cell-adhesive peptides (arginine-glycine-aspartic acid, RGD) before and after gelation. Graphical abstract of the results for cancer cells subjected to (**B**) low confining stress in the sparsely cross-linked soft hydrogel that delays spheroid growth with no/little volumetric expansion ($d_1 \approx d_2$) after stress relief or (**C**) high confining stress in the densely cross-linked stiff hydrogel that enhances spheroid growth with remarkable volumetric expansion ($d_2 > d_1$) after stress relief, respectively.

and the associated stemness markers, which were abolished in cells cultured in the softer hydrogels or with stress relief. The mechano-primed cancer cells exhibited substantial cancer prognosis–related behaviors, including robust tumor growth and metastasis in vivo. Together, our findings provide critical mechanistic insights into the impact of confining stress on tumor growth and development.

RESULTS
Fabrication of hydrogels with varying stiffnesses
We fabricated hydrogels with varying stiffnesses while keeping the content of HA polymer and conjugated cell-adhesive ligands

(arginine-glycine-aspartic, RGD) the same. We synthesized the methacrylated HA (MeHA) with three distinct modification degrees of ~15, ~50, and ~115% via methacrylating primary hydroxyl groups of N-acetyl-D-glucosamine or/and nonprimary hydroxyl groups in glucuronic acid units of HA (fig. S1) (19), which were further coupled with the same amount of RGD according to previous reports (20, 21). The photopolymerization of precursor solutions resulted in the formation of three hydrogels with defined stiffnesses (Fig. 2A): "soft" (2.72 ± 0.59 kPa), "intermediate" (33.27 ± 4.87 kPa), and "stiff" (102.97 ± 16.11 kPa). It is known that tumors develop notably stiffer matrix compared with that of healthy tissues (22, 23). The hydrogel stiffnesses of different
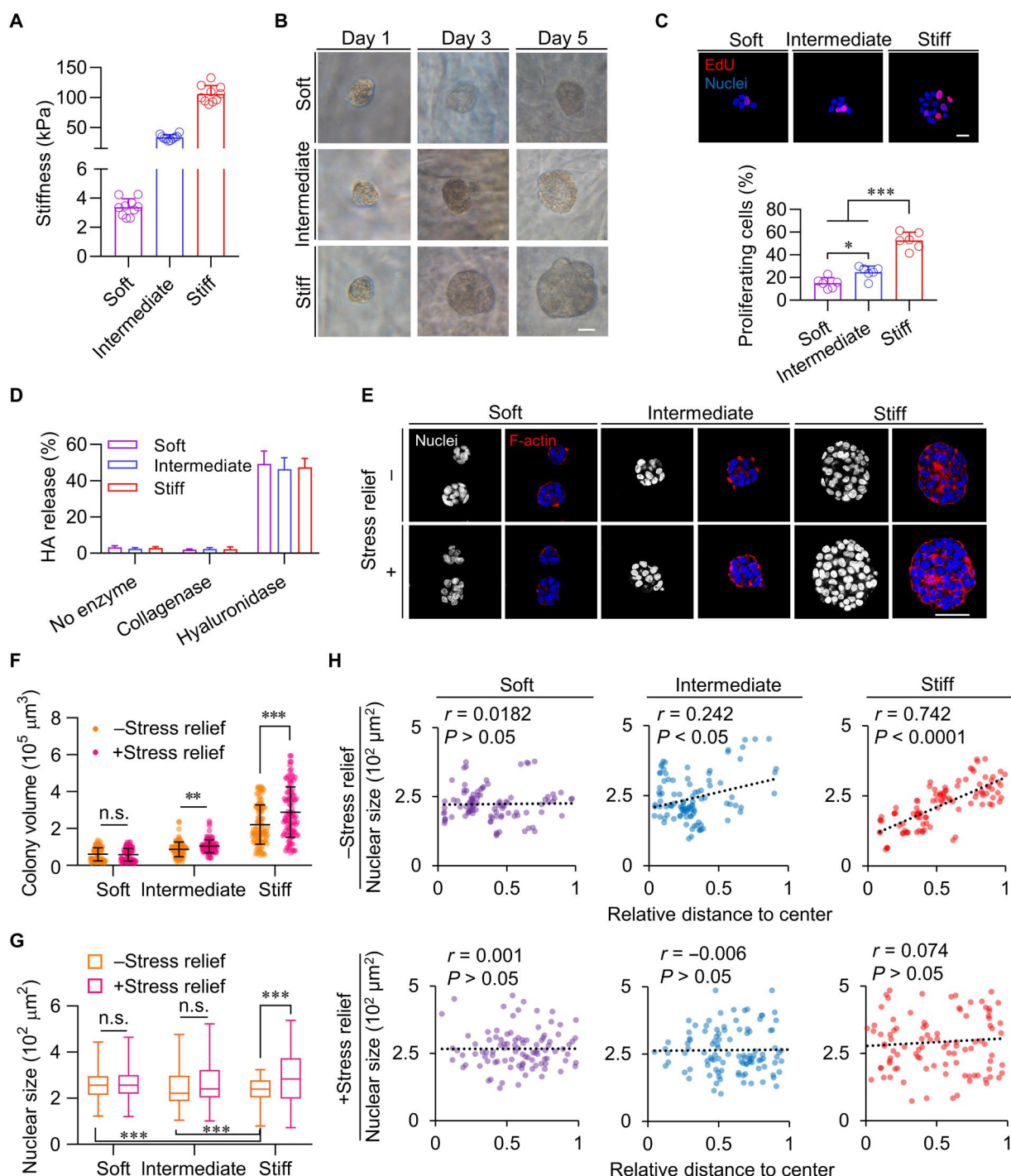
Fig. 2. Cancer cells preferentially grew under highly stressed conditions in the stiff hydrogel. (**A**) Mechanical assessments of MeHA hydrogels with varying rigidity. Each point represents one hydrogel sample ($N = 8$). (**B**) Optical images for single colony growth evaluation of colorectal cancer cells (CRCs) in the hydrogels from day 1 to 5. (**C**) The percentage of proliferating cells by 5-ethynyl-2′-deoxyuridine (EdU) staining assay (each point represents one hydrogel sample, $N = 6$) on day 3. (**D**) Quantification of degraded HA released from the hydrogels containing cancer cells with or without exposure to hyaluronidase or collagenase from day 4 to 5 of incubation. (**E**) Fluorescent images of staining against F-actin (red) and nuclei (blue) of the cancer spheroids on day 5 with or without stress relief applied on day 4. The cancer spheroids in the stiff hydrogel showed the most notable volumetric expansion after stress relief, indicating the highest confining stress before relief. Scale bars, 20 μm [(B), (C), and (E)]. (**F**) Quantification of spheroidal cancer cell colony volume in different groups on day 5 with or without stress relief applied on day 4 ($n = 100$, each point represents one colony from $N = 3$ independent hydrogels). (**G**) Box and whisker plot of nuclear sizes ($n = 100$ nuclei from $N = 3$ independent hydrogel samples) and (**H**) scatter plots of nuclear sizes against the relative radial distance to the cancer spheroid center on day 5 with or without stress relief applied on day 4 ($n = 100$, each point representing an individual nucleus, from $N = 3$ independent hydrogel samples). r presents Pearson's correlation coefficient. Data represent the means ± SD. Significant difference P values: *$P < 0.05$; **$P < 0.01$; ***$P < 0.001$. n.s. denotes no significant difference ($P > 0.05$) [analysis of variance (ANOVA)].

groups in this study were selected on the basis of the stiffness of nonbone healthy tissues (soft) (24), malignant tissues, and cancer models (intermediate and stiff) (7, 25, 26), respectively.

Cancer cells preferentially grow in the highly stiff hydrogel

We obtained tumor cells from a patient with stage 3 colorectal cancers (CRCs) for ex vivo study. We encapsulated single cancer cells in hydrogels with the same seeding density in all groups of hydrogels to minimize initial cell-cell interactions and monitored cell colony growth in groups over 5 days of culture (Fig. 2B and fig. S2). Notably, the average colony size of cancer cells in the stiff hydrogel was ~3.5 times and ~2.5 times that in the soft and intermediate hydrogels, respectively, on day 5 (Fig. 2, B and F). Colonies in all groups remained relatively spherical (fig. S3), suggesting minimal cell migration and minimal hydrogel degradation (fig. S4). The average percentage of proliferating cells cultured in the stiff hydrogel was 247 and 113% higher than that in the soft and intermediate hydrogels, respectively (Fig. 2C), consistent with the enhanced colony growth of cells in the stiff hydrogel (Fig. 2F). In contrast, an ultrastiff hydrogel (396.14 ± 44.73 kPa) slightly reduced colony growth compared to the stiff hydrogel (102.97 ± 16.11 kPa) (fig. S5), suggesting that excessive confinement could inhibit cancer cell proliferation (27). Furthermore, we confirmed that all cells remained highly viable (>90% living cells per colonies) in the soft, intermediate, and stiff hydrogels over 5 days (fig. S6). Thus, we chose the stiff (~100 kPa) as the hydrogel with the highest stiffness for cell culture throughout the study.

The cancer cell lines, including HeLa (human cervical cancer model), Hep3B (human liver adenocarcinoma model), MDA-MB-231 (human breast adenocarcinoma model), MCF-7 (human breast cancer model), and CT26 cells (a murine colorectal carcinoma model), exhibited a similar stiffness-dependent colony growth trend as the CRCs (figs. S7 and S12). These results indicate that the stiff hydrogel can enhance the colony expansion of a wide array of cancer cells. Nevertheless, human mesenchymal stem cells (hMSCs) remained as single-rounded cells over 5 days of culture in all groups (fig. S8), showing that noncancer cells might have other intrinsic pathways that prevent cell growth in a confined space. In contrast, replacing RGD with nonbioactive peptide sequence Asp-Ala-Arg (RAD) or inhibiting β_1/β_3 integrin impeded CRC growth, showing that CRCs required interactions with cell adhesive ligands from the hydrogel for survival (figs. S9 and S10) (28). Collectively, our findings indicate that the stiff hydrogel is conducive to promoting the proliferation of encapsulated cancer cells.

## Cancer organoids developed in stiff hydrogels are subject to increased confining stresses

Intratumoral mechanical stress accumulates during cancer growth and influences cancer cell behavior (5, 29, 30). We investigated whether hydrogel stiffness governs this stress toward the tumor spheroid (31). Thus, we partially degraded the HA hydrogels from day 4 to 5 of culture to soften the hydrogel and induce stress relief to assess the volumetric change of the CRC spheroids as an indirect index of the confining stress profile (Fig. 1, B and C). The hydrogels degraded specifically in the presence of hyaluronidase but not collagenase or no treatment over 8 days of culture (Fig. 2D and fig. S4). The resulting stiffnesses of the partially degraded soft, intermediate, and stiff hydrogels were 0.97 ± 0.28, 14.32 ± 2.78, and 48.81 ± 6.82 kPa, respectively (fig. S11), proving

the efficacy of degradation-induced stress relief. Subsequently, the stiff hydrogel–cultivated CRC and CT26 cell spheroids expanded their colony size by ~30% after degradation-induced hydrogel softening (stress relief), but this volumetric change was minimal in the other two groups (Fig. 2, E and F, and fig. S12). The resulting proliferation rates of CRCs after the stress relief were 11.64 ± 2.31, 16.67 ± 5.20, and 35.66 ± 5.09% for the soft (original: 15.17 ± 4.71%), intermediate (original: 24.74 ± 5.37%), and stiff (original: 52.61 ± 7.35%) hydrogel groups, respectively (fig. S13, A and B). This moderate reduction in cell proliferation rates after stress relief indicates that the cells retained the mechanical memory within the stress relief period (32). To rule out the possibility that cell division contributed to the colony volume expansion during the stress relief period, we added aphidicolin to block the cell cycle at the early S phase during the stress relief (28). Our results showed that the amount of colony volume expansion remained similar in all groups with and without cell division blockade (fig. S13C). To further rule out the potential influence of low molecular weight HA on the cells during enzymatic stress relief, we physically peeled off a hydrogel layer to achieve stress relief for the exposed colonies and observed the morphological change of those CRC colonies after 24 hours (fig. S14A). After this physically induced stress relief, the volume of the exposed colonies in the stiff hydrogel group showed a ~40% increase similar to that found after enzymatic stress relief (Fig. 2, E and F; and fig. S14, B and C). In short, these results suggest that the stiff hydrogel imposed high confining stress on the encapsulated cancer cells.

Intratumoral stress also influences nuclear sizes within spheroids (33). The average nuclear size in CRC spheroids in the stiff hydrogel group was 26.7% smaller than that in the soft hydrogel group (Fig. 2G). The graphical plot of individual nuclear sizes against the relative radial distance to the cancer spheroid center shows a positive correlation between nuclear size and cell position, especially in the stiff hydrogel (Fig. 2H), but no such trend in the soft hydrogel group, consistent with the previous literature (30, 33). After stress relief, the average cell nuclear size in the stiff hydrogel increased by ~20%, while there was no significant change ($P > 0.05$) in the other two groups (Fig. 2G). Furthermore, stress relief abolished the nuclear size gradients within cancer spheroids cultured in both intermediate and stiff hydrogels (Fig. 2H). Our findings suggest that the confining stress also influences nuclear size in cancer spheroids, which can be a marked biomechanical signal to potentiate cancer tumorigenicity.

High confining stress promotes the expression of Hsps to mediate the survival of cancer cells in the stiff hydrogel

To understand the molecular mechanism underlying the enhanced cell growth induced by high confining stress, we used whole-transcriptome sequencing [RNA sequencing (RNA-seq)] to study the expression pattern of Hsps, which may regulate cell survival and proliferation under mechanically stressed conditions (11). Stress-inducible Hsp70 isoforms can be encoded by multiple genes, including Hsp70-1 (HSPA1A), Hsp70-12A (HSPA12A), and Hsp70-hom (HSPA1L), depending on the type of stress signals (34). Critically, these genes were the most up-regulated in the stiff hydrogel compared with that in the softer hydrogels (Fig. 3A), suggesting that mechanical cues can modulate Hsp signaling. Therefore, we first assessed the expression of Hsp70 as the downstream target in the cultivated cells in the first 72 hours for early-stage
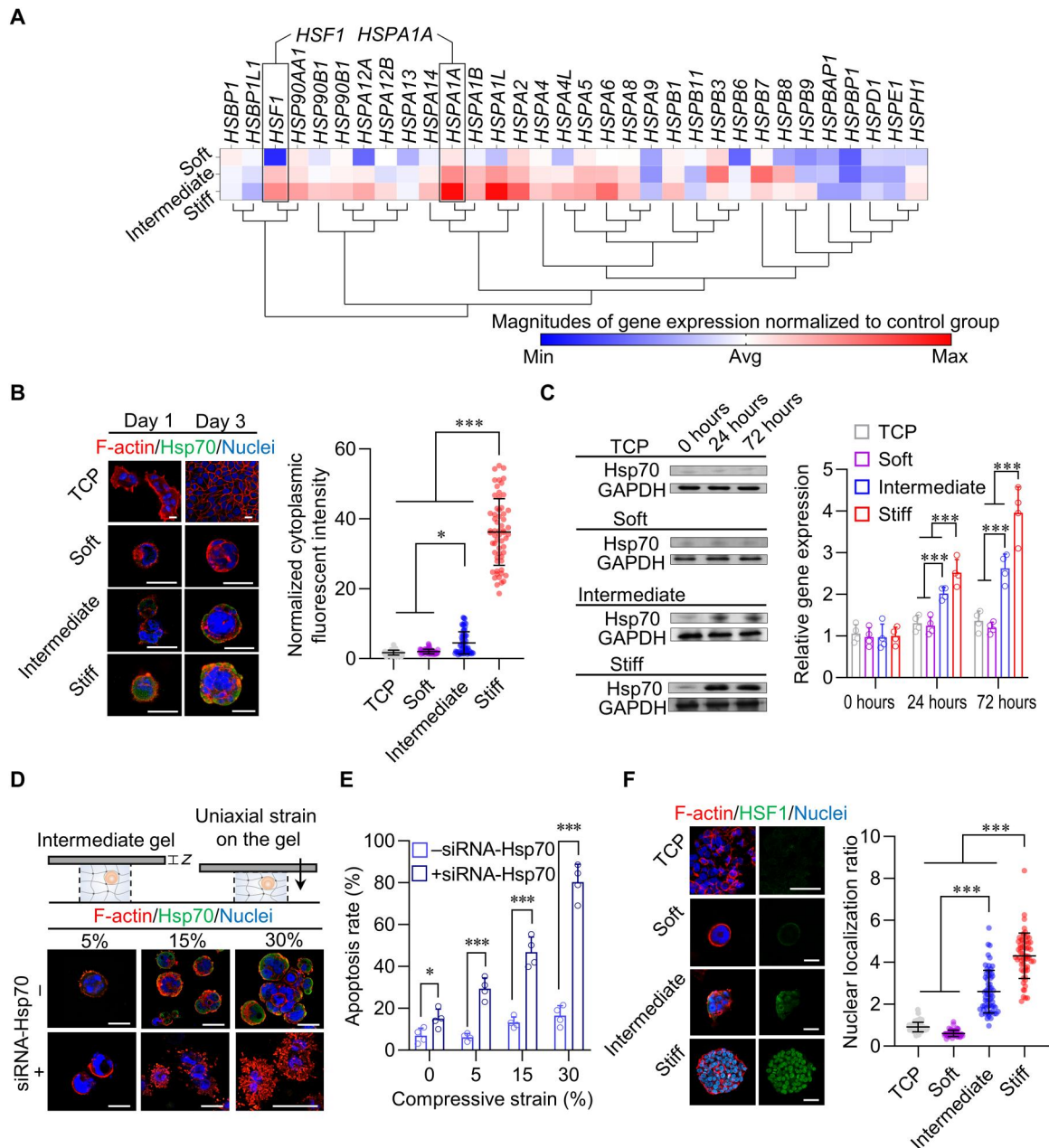
Fig. 3. Hsp70 plays a critical role in cancer cell growth and survival under mechanical stress in the stiff hydrogel. (**A**) Heatmap of heat shock protein (Hsp)–associated gene expression determined by RNA sequencing (RNA-seq) comparing cancer cells in the soft, intermediate, and stiff hydrogels (N = 3). The unit for the color scale was the z score of the log$_2$ expression data shown. All RNA-seq data were normalized to the tissue culture plate (TCP) group. Fluorescent images of staining against (**B**) Hsp70 (green) from day 1 to 3 and (**F**) heat shock factors (HSF-1; green) on day 5 with F-actin (red) and nuclei (blue) in the encapsulated CRCs as well as the fluorescence intensity measurement of Hsp70 on day 3 and nuclear localization ratio of HSF-1 on day 5, respectively (n = 60 colonies from N = 3 independent hydrogels, each point representing one colony). Scale bars, 20 μm [(B) and (F)]. (**C**) Quantification of Hsp70 protein (left) and gene (right) expression by cancer cells in different groups over 72 hours (N = 4, each point representing an independent hydrogel). (**D**) Schematic illustration of uniaxial compression on cancer cells encapsulated in intermediate stiffness hydrogel and images of fluorescence staining against Hsp70 in cancer cells with or without small interfering RNA (siRNA) knockdown of Hsp70 (siRNA-Hsp70) under varying levels of compression on day 3. Scale bars, 25 μm. (**E**) Apoptosis rates of CRCs cultured in the intermediate stiffness hydrogel with or without siRNA-Hsp70 under various magnitudes of uniaxial compression on day 3 (N = 4 independent samples). Data represent the means ± SD. Significant difference P values: *P < 0.05 and ***P < 0.001 (ANOVA).

assessment. We used a tissue culture plate (TCP) as the nonconfined control. Our immunofluorescent staining results revealed that the expression of Hsp70 in the stiff hydrogel group was ~6 times as much as that of the soft hydrogel or TCP group (Fig. 3B). Similarly, the gene expression and protein synthesis of Hsp70 rapidly increased from 0 to 72 hours in cells cultured in the stiff hydrogels (Fig. 3C). We further showed that the up-regulation of Hsp70 was also valid in single cells with cell division blockade over 5 days of culture (fig. S15). Consistently, the five cancer cell lines showed a similar trend of Hsp70 gene expression as that of the CRCs (figs. S16 and S17). In contrast, the CRCs grown on TCP, in the soft hydrogel (Fig. 3C), or stiff hydrogel with stress relief generally expressed a low or decreased level of Hsp70 throughout the culture,
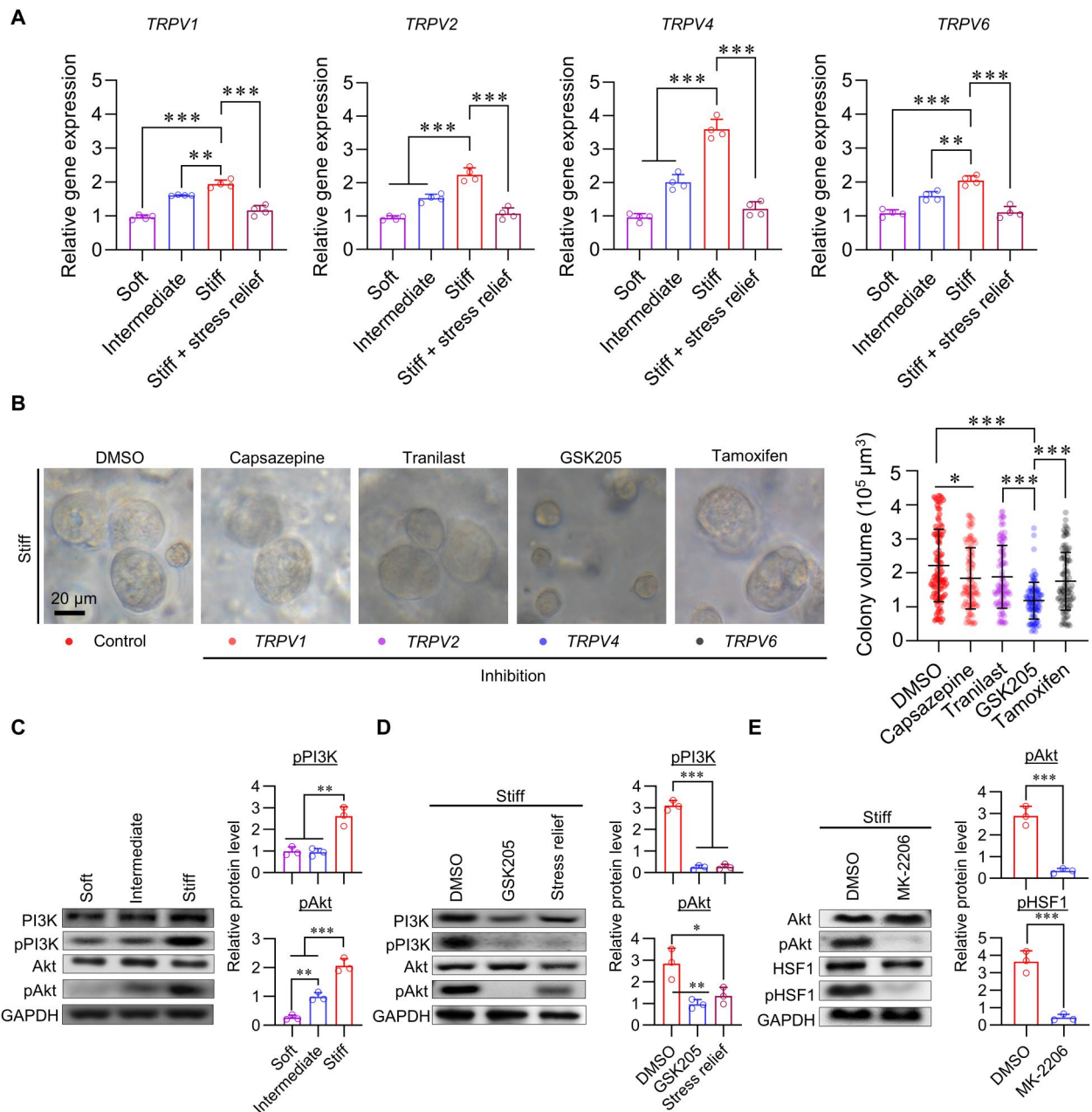
Fig. 4. TRPV4 is the critical mechanosensation link between mechanical stress and activation of HSF1 signaling. (**A**) Quantification of the relative gene expression of transient receptor potential vanilloid (TRPV) family (TRPV1, TRPV2, TRPV4, and TRPV6) in CRCs cultured in various stiffnesses for 5 days ($N = 4$ independent hydrogels). (**B**) Evaluation of the effect of pharmaceutical inhibitions of TRPV family on CRC colony growth in the stiff hydrogel over 5 days with colony size quantifications ($n = 100$ colonies from three individual gels, each point representing one colony from $N = 3$ independent hydrogels). DMSO, dimethyl sulfoxide. (**C** and **D**) The Western blot data of phosphorylation of phosphatidylinositol 3-kinase (pPI3K) and Akt in CRCs cultured in hydrogels with varying stiffnesses, inhibition of TRPV4 (GSK205), or by stress relief, respectively ($N = 3$ independent hydrogels). GAPDH, glyceraldehyde-3-phosphate dehydrogenase. (**E**) The Western blot data of pAkt and HSF1 in CRCs cultured in the stiff hydrogel with or without Akt inhibition by MK-2206 ($N = 3$). Data represent the means ± SD. Significant difference P values: *$P < 0.05$; **$P < 0.01$; ***$P < 0.001$ (ANOVA).

respectively (fig. S18) (*35*), confirming that the stiff hydrogel up-regulates Hsp70 expression in cancer cells.

We postulated that a compressed hydrogel softer than a stiff hydrogel could partially recreate a high confining stress environment for cancer cells. We applied defined levels of uniaxial compression on the intermediate hydrogel encapsulating CRCs by a micromechanical system over 3 days (Fig. 3D) (*36*). The expression of Hsp70 in the CRCs gradually increased with increasing static compressive strain (fig. S19B). The Hsp70 expression reached its highest level at 30% strain, with a subsequent decrease when compression was increased from 30 to 35%, probably due to hydrogel fracture. Increasing the applied compression strain (<35%) also promoted cancer colony growth (fig. S19A). Treatment with small interfering RNA (siRNA)–Hsp70 not only attenuated the Hsp70 expression of the cancer cells (fig. S25) but also promoted the cellular apoptotic rate under increased mechanical compression (Fig. 3, D and E). The results further highlight the critical role of Hsp70 in promoting cancer cell survival and growth in hydrogels under high confining stress.

Stiff hydrogel–imposed mechanical stimulation up-regulates Hsp70 expression by activating the upstream TRPV4-PI3K/Akt-HSF1 signaling axis

The expression of Hsp70 is regulated by the phosphorylation of HSF1 (pHSF1), a key transcription factor of Hsp that translocates to the nucleus and initiates the transcription of Hsp70 (*37*). Our immunofluorescence staining results indicated that HSF1 was highly localized in the nuclei of the CRCs cultivated in the stiff hydrogel but had a much higher cytosolic distribution in those cultivated in the softer hydrogels or cultured on TCP (Fig. 3F). Consistently, the pHSF1 protein was more highly expressed in the stiff hydrogel group than in the other groups (fig. S20, A and B). siRNA knockdown of HSF1 pronouncedly down-regulated the protein expression of Hsp70 in cells cultured in the stiff hydrogel (fig. S20, C and D). Stress relief substantially reduced the nuclear localization of HSF1 in the stiff hydrogel group (fig. S21). These results suggest that HSF1 is a mechanosensitive transcription factor and is critical in regulating Hsp70 expression in cancer cells.

Cumulative evidence has revealed that pHSF1 is regulated by the PI3K/Akt pathway (*38*, *39*), which can be further governed by upstream pathways, including TRPV4, which links mechanical cues and intracellular signaling (*27*, *40*). To examine this signaling axis, we first evaluated the overall activity of four TRPV family members (TRPV1, TRPV2, TRPV4, and TRPV6) that can be associated with the biophysical cues of TMEs (*41*). Generally, the gene expressions of all TRPV members in CRCs were up-regulated along with increased hydrogel stiffnesses, especially for TRPV4 in the stiff group with more than twofold increase compared to the soft group (Fig. 4A). This result suggests that mechanical confinement can noticeably influence the activation of membrane receptors that are mechanosensitive. Next, we performed a corresponding pharmaceutical inhibition on those TRPV members in the stiff hydrogel group. Inhibiting TRPV4 markedly reduced the colony volume, while the colony volumes in other groups only slightly decreased (Fig. 4B), indicating TRPV4 as the most important mechanotransducer for the downstream pathways, including PI3K/Akt signalings. As expected, PI3K and Akt (Tyr^{326}) phosphorylations were much promoted with increasing hydrogel stiffness (Fig. 4C). However, stress relief or the addition of the TRPV4 antagonist (GSK205) markedly inhibited PI3K and Akt phosphorylation in the stiff group (Fig. 4D), indicating that confining stress mediates the activation of the TRPV4-PI3K/Akt signaling axis. Furthermore, Akt inhibition by MK-2206 suppressed pHSF-1 protein expression in cells cultured in the stiff hydrogel (Fig. 4E). Consistent with the result of pharmacological treating TRPV4, inhibiting Akt and Hsp70 signaling activity substantially reduced CRC colony sizes (fig. S22). As a parallel study, we confirmed that the mechano-primed CT26 cells highly expressed TRPV4 (fig. S23A), while the pharmaceutical inhibition of TRPV4 or Akt resulted in a similarly low Hsp70 expression as that achieved by directly inhibiting Hsp70 (fig. S23B). Together, we demonstrate that confining stress can regulate Hsp70 expression by activating the upstream TRPV4-PI3K/Akt-HSF1 signaling axis to promote cancer cell growth and survival under stress conditions.

Stiff hydrogel up-regulates the stemness marker expression of cancer cells via Hsp70/Hsp90-mediated STAT3 phosphorylation

Previous studies have implicated the Hsp70/Hsp90 complex in both the acquisition and maintenance of stem cell "stemness" (*42*) by interacting with signal transducer and activator of transcription 3 (STAT3; Fig. 5A) (*43*–*45*). Our study showed that the stiff hydrogel group exhibited robust protein expressions of both Hsp70 and Hsp90, which were much lower in the softer hydrogel and TCP groups (Fig. 5C). Critically, only the stiff hydrogel–cultivated cancer cells showed pronounced phosphorylation (pSTAT3) and nuclear translocation of pSTAT3 (Fig. 5, B and D). Furthermore, stress relief in the stiff hydrogel reduced the pSTAT3 nuclear localization ratio by ~60% (fig. S24). Because heat shock stress is the classic cause of the elevated expression of Hsp, we cultured cancer cells on TCP at 42°C for 60 min as the positive control to examine how Hsp influences STAT3 signaling (*46*). This heat shock stress elevated the expression of both Hsp70 and Hsp90 and the nuclear localization of pSTAT3 (Fig. 5, B to D), similar to those in the stiff hydrogel group. siRNA-mediated knockdown of either Hsp70 or Hsp90 did not interfere with the protein expression of each other but markedly down-regulated pSTAT3 in the stiff hydrogel group (Fig. 5, B and D, and fig. S25). These results illustrate that Hsp70 and Hsp90 play a cooperative role in regulating pSTAT3 in cancer cells under high confining stress.

To confirm the crucial role of STAT3 in promoting cancer cell stemness, we examined the expression of Nanog (Fig. 5E), which also governs the expression of other stemness-related markers, such as octamer-binding transcription factor 3/4 (Oct3/4) and sex-determining region Y-box2 (Sox2), in different groups (*47*). Consistently, only cells cultured in the stiff hydrogel exhibited pronounced gene and protein expression of these markers (fig. S26), especially Nanog, which was highly localized in the nuclei of stiff hydrogel–cultivated cells (Fig. 5F) but abrogated by the pharmaceutical inhibition of STAT3 phosphorylation by Stattic, siRNA-based knockdown of Hsp70/Hsp90, or stress relief in the stiff hydrogel group (Fig. 5, G and H). Similarly, Nanog was mostly expressed in CT26 cells cultured in the stiff hydrogel (fig. S27). These findings indicate that the elevated expression of Hsp70/Hsp90 and pSTAT3 due to high confining stress contributes to the enhanced cancer cell stemness in the stiff hydrogel.
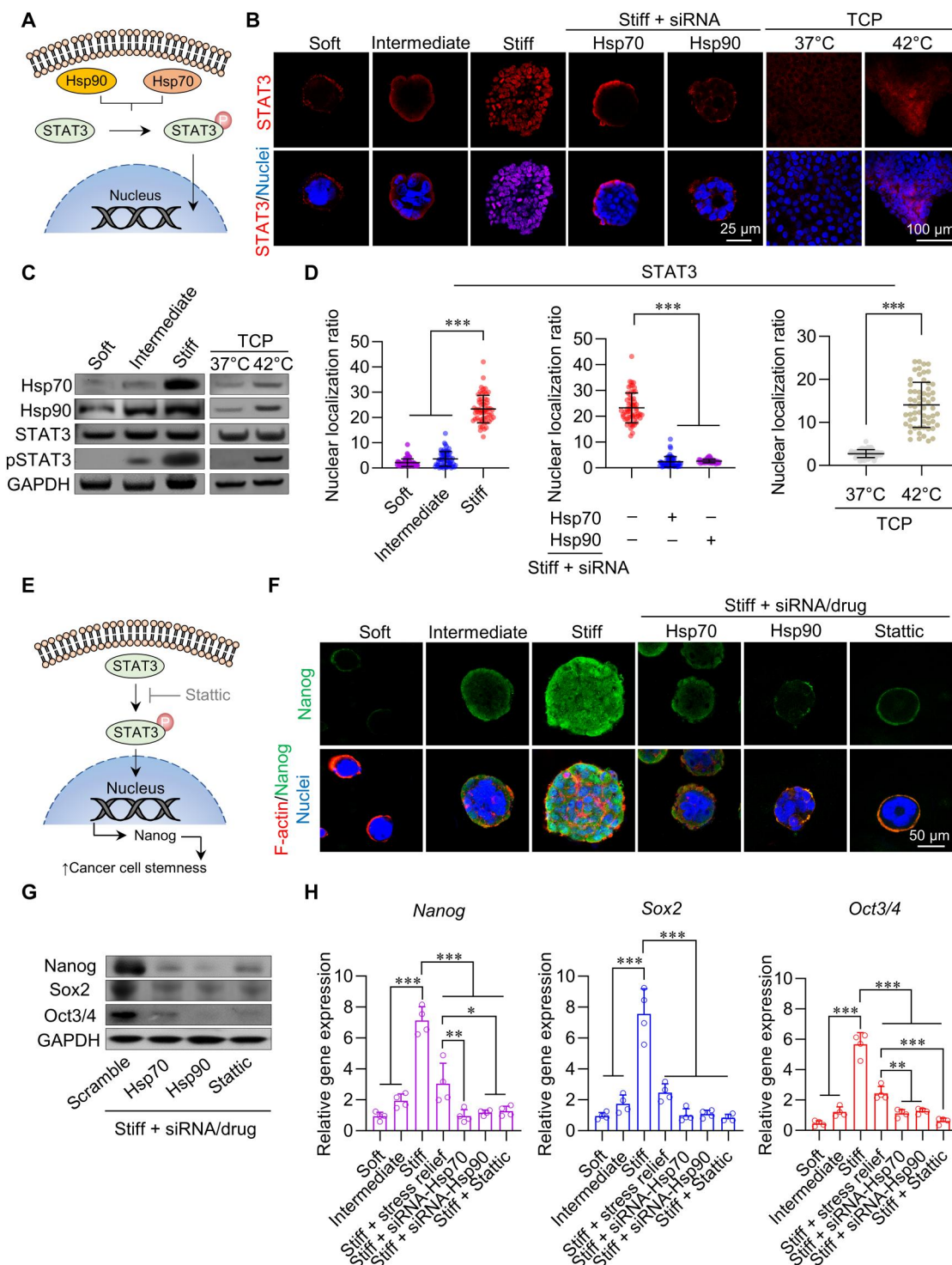
Fig. 5. The elevated expression of Hsp70 due to mechanical stress enhances cancer cell stemness in the stiff hydrogel. (**A**) Schematic illustration of the Hsp70/Hsp90 association assisting phosphorylation of signal transducer and activator of transcription 3 (pSTAT3). (**B**) Images of immunofluorescence staining against STAT3 (red) and nuclei (blue) in CRCs cultured under various conditions. (**C**) The Western blot data of Hsp70, Hsp90, STAT3, and pSTAT3 in different groups. (**D**) Quantification of the nuclear localization of STAT3 in (B). ($n = 60$, each point represents one nucleus from $N = 3$ independent hydrogels). (**E**) Schematic illustration of the transcriptional regulation of Nanog expression by pSTAT3 and its pharmacological blockade by Stattic. (**F**) Images of immunofluorescence staining against Nanog (green), F-actin (red), and nuclei (blue) in CRCs cultured under various conditions. (**G**) The Western blot data and (**H**) relative gene expression of Nanog, sex-determining region Y-box2 (Sox2), and octamer-binding transcription factor 3/4 (Oct3/4) in different groups. ($N = 4$, each point represents an independent hydrogel). All experiments were assessed on day 5 of culture. Stress relief was performed from day 4 to 5. Data represent the means ± SD. Significant difference P values: *$P < 0.05$; **$P < 0.01$; ***$P < 0.001$ (ANOVA).

Stiff hydrogel–derived cancer cells exhibit substantially enhanced tumorigenic and metastatic potential

Because HSPA1A was the eighth most up-regulated gene in the stiff hydrogel group (Fig. 6A and table S1) and cancer cell stemness is associated with cancer tumorigenicity and malignancy (48), we examined the differentially expressed genes (DEGs) in RNA-seq and Kyoto Encyclopedia of Genes and Genomes (KEGG) enrichment

pathways of the cancer cells cultured in the (i) soft hydrogel, (ii) stiff hydrogel, and (iii) stiff hydrogel treated with siRNA-Hsp70 (stiff + siRNA-Hsp70). Principal components analysis suggested that the global gene expression of the stiff hydrogel group was much different from that of the other groups (fig. S28, A and B). For relevance to human diseases, the number of up-regulated DEGs in the stiff hydrogel revealed marked enrichment in the

Fig. 6. Hsp70 is the key mechanosensitive mediator contributing to the enhanced in vivo tumorigenic and metastatic potential of CRCs primed with mechanical stress in the stiff hydrogel. (**A**) Volcano plots for differentially expressed genes (DEGs). Gray, non-DEGs; red, up-regulated DEGs; blue, down-regulated DEGs. FDR, false discovery rate. (**B**) Bubble chart of oncology-related Kyoto Encyclopedia of Genes and Genomes (KEGG) enrichment pathways of DEGs in different groups. The size of the bubbles represents the rich ratio, denoted by the number below the bubble. (**C**) Schematic illustration of CRCs pretreated in hydrogels over 5 days and subsequent isolation for subcutaneous or tail vein inoculation into nude mice for in situ–grown tumor model creation over 20 days or for metastatic lung tumor model creation over 2 months with survival time examination, respectively (N = 6 independent mice). Drugs [JG98 and/or doxorubicin (DOX) at 10 mg/kg] or phosphate-buffered saline (PBS) were injected via the tail vein on day 10 after inoculation in both models. (**D**) Individual growth curves of tumors in animals inoculated by groups (a) to (f), corresponding to each treatment or culture condition. (**E**) Statistical analysis of end point (day 20) tumor volumes (N = 6 independent mice). (**F**) Survival curves for each treatment arm and in different groups [N = 6 independent mice, log-rank (Mantel-Cox) test]. (**G**) Hematoxylin and eosin staining of histological sections of the in situ–grown tumor on Day 20 and lung tumor models on day 30 in different groups. Scale bars, 100 μm. (**H**) Quantification of the relative gene expression of Nanog in tissues harvested from the in situ–grown tumors on day 20 (N = 6 independent mice). Data represent the means ± SD. Significant difference P values: *P < 0.05; **P < 0.01; ***P < 0.001. n.s. denotes no significant difference (P > 0.05) (ANOVA).
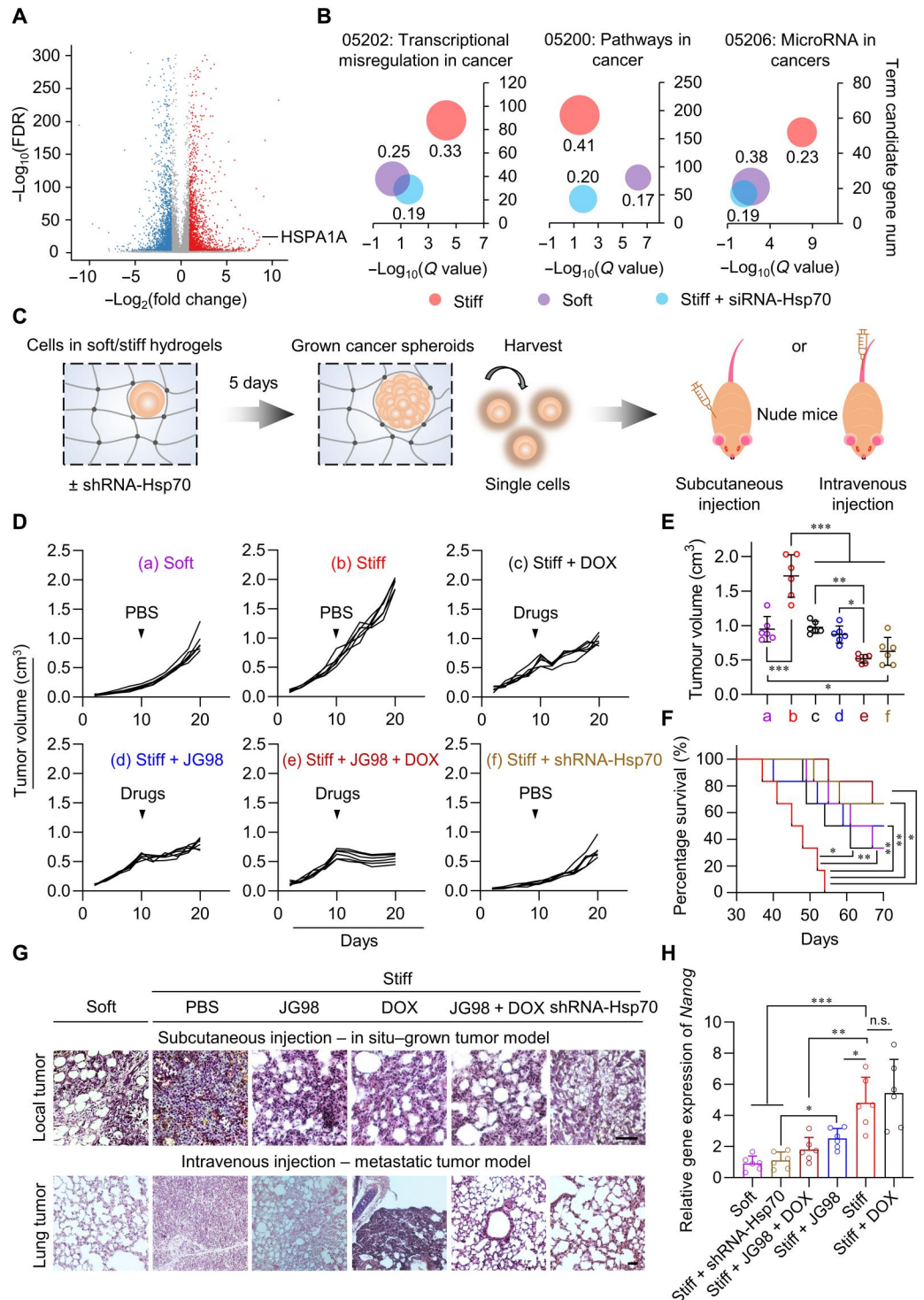
nine top up-regulated KEGG pathways, including 05202: transcriptional misregulation in cancer, 05200: microRNAs in cancer, and 05206: pathways in cancer (Fig. 6B, fig. S28C, and table S2). These pathways are critical to the prognosis of cancer cells, such as survival and migration (49–51). However, the number of enriched genes was reduced by more than 50% in the soft hydrogel and stiff + siRNA-Hsp70 groups (table S2), suggesting the crucial impact of Hsp70 on oncology-related pathways.

Cells develop mechanical memory of past exposure to biophysical signals, and their future cellular behaviors can be potentially predicted in another environment (32). Hence, the mechanoprimed CRCs in vitro may retain the acquired tumorigenic features associated with Hsp70 in vivo (Fig. 6C). Notably, we included a negative control of CRCs primed with Hsp70 silencing [short hairpin RNA (shRNA)–Hsp70] before the in vivo study (Fig. 6C). We also intravenously administered doxorubicin (DOX; stiff + DOX) and/or the Hsp70 inhibitor, JG98 (stiff + JG98) 10 days after CRC injection to evaluate the effect of chemotherapy and/or Hsp70 inhibition in the stiff group. Tumors overgrew (~2 cm^3) from only 10,000 stiff hydrogel–derived CRCs 20 days after inoculation (Fig. 6, D, E, and G), and the size of tumors in the stiff hydrogel group was twice as much as that in the soft hydrogel group. The shRNA-Hsp70 group exhibited the slowest tumor growth (end point tumor size: ~0.6 cm^3), consistent with the in vitro study (fig. S22). Notably, combined treatment (stiff + DOX + JG98) was more effective than the separate treatment (stiff + DOX or stiff + JG98) in reducing this growth (Fig. 6, D to F), suggesting that the inhibition of Hsp70 sensitized CRCs to apoptosis induced by chemotherapy drugs, as Nanog is a chemoresistant stemness marker (28, 52). However, the tumor growth of the soft group was only delayed by the administration of DOX but was not further delayed by the effect of JG98 (fig. S29). Our results indicate that the groups with low Hsp70 expression/activity, including soft, stiff + shRNA-Hsp70, and stiff + JG98 (fig. S30), all had low Nanog gene expression (Fig. 6H). Hence, these findings show the importance of Hsp70-mediated stemness of mechanically primed CRCs in robust tumor formation and the potential value of targeting Hsp70 to enhance the therapeutic outcomes of chemotherapy.

Next, we examined the cancer metastasis and survival of mice after intravenous injection of the hydrogel-derived CRCs. Both the stiff + shRNA-Hsp70 and stiff + DOX + JG98 groups showed the highest survival rate compared with that in the nontreated stiff hydrogel group, which had the shortest survival time among all groups (Fig. 6, F and G). Moreover, 7 to 8 of 10 nude mice developed lung metastasis in the stiff + DOX and stiff groups, while only 1 to 3 of 10 nude mice in the TCP soft or stiff + shRNA-Hsp70 groups showed signs of lung metastasis (table S3). Consistently, only the stiff and stiff + DOX groups exhibited the highest Hsp70 expression in the lungs (fig. S30), suggesting that the metastatic potential of CRCs derived from the stiff hydrogel was associated with elevated Hsp70 activity. Together, these results indicate that the confining stress–induced expression of Hsp70 in CRCs enhances tumorigenicity and metastasis in vivo upon transplantation in mice.

DISCUSSION
In this work, we showed that the high confining stress imposed by the stiff hydrogels enhanced the survival, proliferation, and stemness of the encapsulated CRCs and other cancer cell lines by up-regulating Hsp70 via the TRPV4-PI3K/Akt-HSF1 signaling axis

(Fig. 7A). We further showed that the elevated protein expression of Hsp70 coupled with Hsp90 promoted pSTAT3 to increase the expression of stemness-related markers. Our animal experiments showed that the cancer cells derived from the stiff hydrogel exhibited substantial tumorigenic (Fig. 7B) and metastatic potential (Fig. 7C). Our findings imply that tumor initiation and progression are highly mechanosensing dependent that Hsp70 can be a promising molecular therapeutic target in cancer treatment. Mechanistically, Hsp-related molecules are strongly associated with the level of stemness in cancer cells.

MATERIALS AND METHODS
Methods
Primary CRC harvesting
CRCs were harvested from a patient with stage 3 (73-year-old male patient). Informed consent was obtained from the recruited patient, and this sample collection protocol was approved by the Joint Chinese University of Hong Kong–Hospital Authority New Territories East Cluster Clinical Research Ethics Committee (human tissue ethics project no.: CREC ref. no.: 2018.500, Department of Surgery at Sir Yue Kong Pao Centre for Cancer, The Chinese University of Hong Kong). A diagnosis of CRC was confirmed by histology and staged at pT3M0N0. Immediately after resection, specimens were dissociated into single cells by a semiautomated combined mechanical/enzymatic process using gentleMACS Dissociator and a Tumor Dissociation Kit, human, according to the manufacturer's instruction (Miltenyi Biotec). Briefly, tumor samples were cut into 5-mm pieces and incubated into C Tube containing enzymes H, R, and A (available in kit) for the mechanical dissociation (rotation for 30 min at 37°C). After that, cells were filtered with EASYstrainer 100 μm (Dutscher) to obtain a single-cell suspension. Last, CRCs were sorted by flow cytometry via identifying CD45(⁻)CD326(⁺)CD90(⁻) to remove immune cells and stromal cells, according to the previous report (53). The tumor cells were expanded up to P1 for the in vitro and in vivo studies.

Encapsulation of cancer cells within MeHA hydrogels for mechanistic study
Previously described methods were used to fabricate MeHA (18) with ~15, ~50, and ~115% methacrylation from sodium hyaluronate (weight-average molecular weight of 40 to 70 kDa; Lifecore). The chemical structures of the modified HA polymers were evaluated by ^{1}H nuclear magnetic resonance (Bruker) spectra. A total of 7.2 mg GCGYGRGDSPG or nonbioactive GCGYGRADSPG (GenScript) was coupled with 100 mg of MeHA overnight reaction in pH 8.0 at 25°C for presenting integrin binding moiety with subsequent lyophilization. Primary CRCs or cancer cell lines including HeLa [the American Type Culture Collection (ATCC), cat. no. CCL-2, RRID:CVCL_0030], MDA-MB-231 (ATCC, cat. no. HTB-26, RRID:CVCL_0062), MCF-7 (ATCC, cat. no. HTB-22, RRID:CVCL_0031), Hep3B (ATCC, cat. no. HB-8064, RRID:CVCL_0326), CT26 cells (ATCC, cat. no. CRL-2638, RRID:CVCL_7256), or passage 3 hMSC (male; Lonza) were encapsulated into MeHA hydrogel (10^6 cells ml^{-1}) using photoinitiated free radical polymerization (EXFO/OmniCure S1000 lamp with a 320- to 390-nm filter, exposure of 10 mW cm^{-2} for 5 min) with 0.05 weight % Irgacure 2959 (I2959, Ciba), a photoinitiator chosen for its aqueous solubility and good cytocompatibility (19). The initial cell seeding density was kept the same among all groups
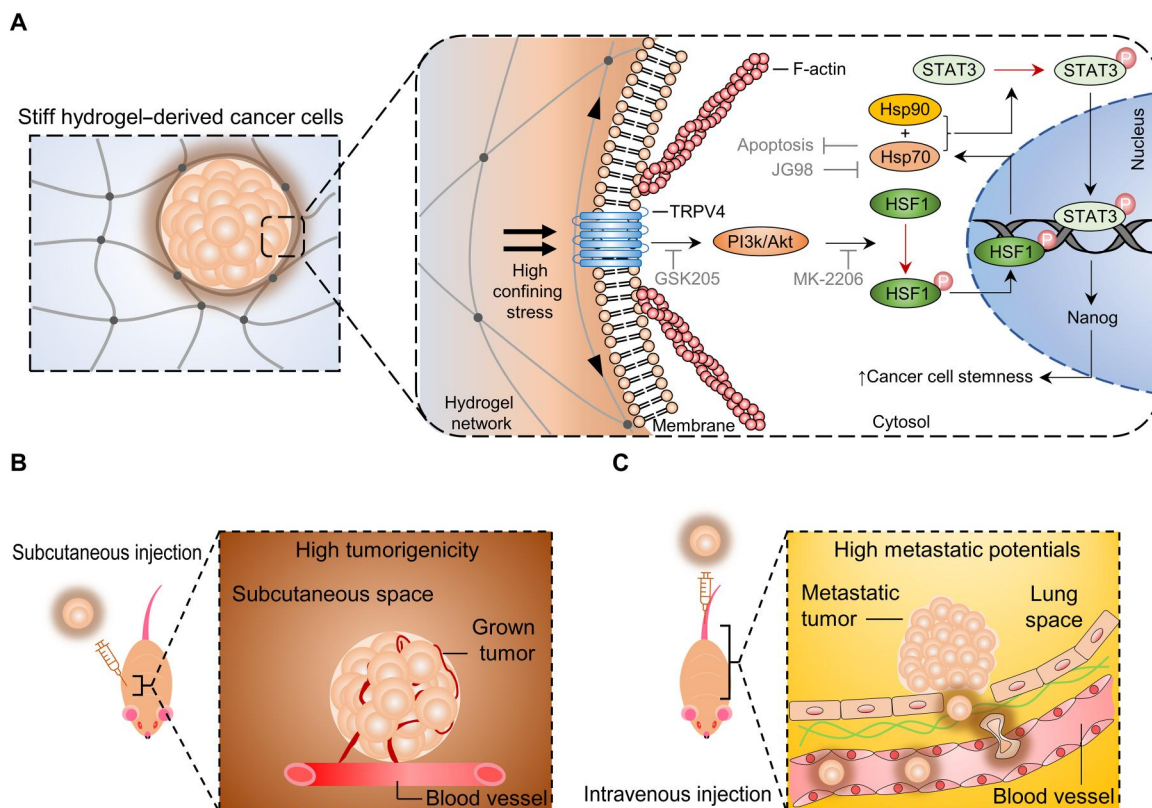
Fig. 7. The proposed schematic summary of the confining stress–activated Hsp70 signaling to promote the survival, proliferation, and stemness of the cancer cells encapsulated in the stiff hydrogel. (**A**) The stiff hydrogel imposes high confining stress on the encapsulated cells, leading to the activation of the stretch-activated channel TRPV4 and the associated PI3k/Akt signaling. The activation enhances the phosphorylation and nuclear localization of HSF1, which promotes the expression of Hsp70 to resist anoikis and apoptosis under mechanical stress. Subsequently, the abundant cytosolic Hsp70 associates with Hsp90 to bridge the nuclear localization of STAT3 through enhanced pSTAT3 that promotes the transcription of Nanog and enhances cancer malignancy. The mechanoprimed cancer cells exhibit (**B**) high tumorigenicity and (**C**) high metastatic potential after subcutaneous or intravenous inoculation, respectively.

of hydrogels. The elastic modulus of the hydrogels was measured by parallel-plate compression testing at 10% ramped strain min^{-1} as previously reported (*18*). All gels encapsulating cells were transferred to growth media supplemented with Dulbecco's modified Eagle medium (Thermo Fisher Scientific), 10% fetal bovine serum (Invitrogen), 1 mM L-glutamine (Invitrogen), 1 mM sodium pyruvate (Invitrogen), and 0.1 mM penicillin/streptomycin (Invitrogen) at 37°C and 5% CO_2. Media changes were performed every 3 days. For the compressive stress study, the cell-containing gel was in a 35-mm^2 culture dish (Corning) in Mach-1 Micromechanical System (Biomomentum Inc., model no. MA005) at 37°C and 5% CO_2. Uniaxial unconfined strain (ε) from 0.05 to 0.35 was imposed onto the gel with a flat indenter of 25.4 mm in diameter. The duration of compression for all cellular uptake experiments was fixed over 72 hours and fixed for further analysis.

Hydrogel degradation and stress relief and assay
After photoinduced gelation with cell encapsulation, the gels were transferred to hyaluronidase (Tokyo Chemical Industry) or collagenase (0.5 mg/ml; Thermo Fisher Scientific) in growth media over 8 days. The sample supernatants (frozen and stored at −20°C after collection) were analyzed in triplicate via a modified uronic acid assay, as previously reported (*54*), to evaluate the percentage of MeHA hydrogel degradation. For stress relief, hyaluronidase or collagenase (0.5 mg/ml) was added to the culture medium on day 4 of

the culture until day 5 for further analysis. Mechanical tests were performed to measure the hydrogel stiffness before and after the stress relief.

Cancer cell colony size, number, and circularity analysis
The images of cancer cell colonies were captured by optical microscopy (Nikon) at different time points. Three different gels were analyzed for each group. The number, size, and roundness (circularity) of cancer cells encapsulated in gels of various stiffnesses were analyzed by ImageJ [National Institutes of Health (NIH)] from the captured images according to the previous report (*54*).

RNA interference, silencing, and integrin blocking experiments in vitro
Cells were seeded into six-well plates at a density of 2.0×10^5 cells per well. The next day, the medium was changed, and the cells were transfected with validated MISSION HSPA1A siRNA (SASI_Hs01_00051449; Sigma-Aldrich), siRNA HSP90AA1 (ID:121532, Thermo Fisher Scientific), HSF1 siRNA Oligos set (NM_005526; Applied Biological Materials Inc.), or negative control (MISSION siRNA Universal Negative Control; SIC-001; Sigma-Aldrich), each at a final concentration of 50 nM in Lipofectamine 3000 (Thermo Fisher Scientific), according to the manufacturer's instructions. The plates were cultured for 48 hours, following which the cells were trypsinized and encapsulated in gels of various stiffnesses over different time points. For Hsp70 silencing, cells were

transfected with a lentiviral vector containing a shRNA sequence (5′-GGACGAGTTTGAGCACAAG-3′), targeting Hsp70 or lentiviral vector backbone as a negative control according to the manufacturer′s protocol (Shanghai Genechem Co. Ltd.) for 12 hours, and the growth media was refreshed with further incubation for 36 hours. Successfully transfected cells were screened by puromycin (Invitrogen) and harvested for hydrogel studies. For integrin (β_1- or β_3-class) inhibition studies, cells were treated with blocking antibodies [5 μg ml^{-1}; β_1-integrin (Santa Cruz Biotechnology, cat. no. sc-374429, RRID:AB_11012020) and β_3-integrin (Santa Cruz Biotechnology, cat. no. sc-52685, RRID:AB_629164)] or isotype control antibody as control [normal mouse immunoglobulin G (IgG), 5 μg ml^{-1}; Santa Cruz Biotechnology, cat. no. sc-2025, RRID:AB_737182] for 24 hours before culturing the cells in the gels in growth media daily during incubation periods. For pharmaceutical inhibition, JG98 (Hsp70 inhibitor; AdooQ Bioscience) of final concentration at 5 μM, Stattic (STAT3 phosphorylation inhibitor; AdooQ Bioscience) of final concentration at 10 μM, MK-2206 (Akt inhibitor; Selleck) of final concentration at 20 μM, capsazepine (TRPV1 inhibitor; Selleck) of final concentration at 20 μM, rranilast (TRPV2 inhibitor; Selleck) of final concentration at 20 μM, GSK206 (TRPV4 inhibitor; Sigma-Aldrich) of final concentration at 20 μM, or tamoxifen (TRPV6 inhibitor; Selleck) was incubated with cells for 24 hours before or during the period of culture in hydrogel encapsulations.

Cell proliferation assay

Cell proliferation assay was assessed by 5-ethynyl-2′-deoxyuridine (EdU) 555 cell proliferation test kit (Beyotime) according to the manufacturer′s instructions. Briefly, cells were incubated with 10 μM EdU working solution for 2 hours at 37°C, followed by fixing with 4% paraformaldehyde (PFA; J&K Chemical), permeabilizing with 0.3% Triton X-100 (Sigma-Aldrich), blocked by 1% bovine serum albumin (Sigma-Aldrich) in phosphate-buffered saline (PBS) at pH 7.4, and lastly incubating with the click reaction solution for 30 min in the dark and staining with 1:5000 Hoechst 33342 (Thermo Fisher Scientific) for 10 min. The cells were washed with PBS and were observed under confocal microscopy. The percentage of proliferating cells for each group was measured by counting the number of EdU positively stained cells over the total cell number. Three independent hydrogels were counted for each group.

Apoptosis assay

The measurement of apoptosis was performed by staining the cells with propidium iodide/annexin V−fluorescein isothiocyanate for flow cytometry analysis. The cells were processed as previously described (55), and cytometric analysis was performed in a BD FACSVia flow cytometer (BD Biosciences); the results were analyzed using Flowing software.

Immunofluorescent staining and imaging

Cells in hydrogels or on culture plates were fixed with 4% PFA for 30 min and permeabilized with 0.01% Triton X-100 (Sigma-Aldrich) for 5 min and blocked by 3% BSA for 1 hour in PBS at pH 7.4. The samples were incubated with mouse monoclonal or rat monoclonal IgG anti-Hsp70 (1:200; Santa Cruz Biotechnology, cat. no. sc-66048, RRID:AB_832518), anti-HSF1 (1:200; Santa Cruz Biotechnology, cat. no. sc-13516, RRID:AB_627751), anti-STAT3 (1:800; Abcam, cat. no. ab68153, RRID:AB_2889877), and anti-Nanog (1:800; Abcam, cat. no. ab109250, RRID:AB_10863442) for overnight at 4°C. The samples were washed with PBS for three times and incubated with secondary antibody Alexa Fluor 488

(Invitrogen, cat. no. A11001) or Alexa Fluor 568 (Invitrogen, cat. no. A11004) goat anti-mouse or Alexa Fluor 488 goat anti-rat (IgG; 1:800; Invitrogen, cat. no. A11006) and Alexa Fluor 488 or Alexa Fluor 568−phalloidin (1:100; Cytoskeleton, Inc) for 2 hours at room temperature. The cell nuclei were stained by DAPI (4′,6-di-amidino-2-phenylindole; 1:1000). The samples were observed and imaged under confocal microscopy.

Mice model

On the basis of a 30% estimated difference between the experimental group (hydrogel of various stiffnesses) and the control groups (TCP or saline injection group), a statistical power (1-β) of 80% at the significance level of α = 5% can be obtained with a minimum sample size of $n = 6$ per group. The Animal Subjects Ethics Subcommittee of the Hong Kong Polytechnic University approved all the experiments listed below (20-21/166-BME-R-GDG). Tumorgenicity of the mechanoprimed cancer cells was examined by performing a subcutaneous injection of cells (10^4 cells) into 6- to 7-week-old Balb/c nude mice (male or female). The daily tumor size was monitored by a digital caliper over 20 days, and the end point tumors were extracted, weighted, and fixed by 4% PFA for further analysis. To evaluate the metastatic potential of the mechanoprimed cancer cells, the cells (10^4 cells) were injected into the tail vein of 6- to 7-week-old nude mice (male or female). The cells cultured in hydrogels of various stiffnesses were harvested via the combination of trypsin and hyaluronidase at 37°C and 5% CO_2, as well as pipetting, to isolate single cells from colonies with filtered by Falcon Cell Strainers (40 μm; Thermo Fisher Scientific) before tumor inoculation. The whole process was finished within 10 min. After 2 months, the weight of the mice was measured, and the organs of the mice were extracted for weight measurement and analysis. For survival evaluation, the date of mice death was recorded over 70 days for each group. For pharmacological treatments, the conditioned group was treated by drug(s), including JG98 and/or DOX at 10 mg/kg on day 10 after tumor cell inoculation.

Hematoxylin and eosin staining and immunohistochemistry of embedded samples

The paraffin-embedded sample of organs and tumors was deparaffinized by xylene (J&K Chemical) and ethanol and rehydrated. To evaluate the overall tissue morphology, the samples were directly stained with hematoxylin (Sigma-Aldrich) solution for nuclei and then washed by the following sequence: tap water, acid alcohol (Beyotime), tap water, Scott′s buffer (Beyotime), and water. Furthermore, the samples were stained with 1% eosin Y alcoholic (Sigma-Aldrich). Last, the samples were gradually dehydrated by ethanol and xylene and mounted by a coverslip. For immunohistochemistry staining, the sample was treated for antigen retrieval by boiling citrate solution (J&K Chemical) buffer at pH 6.0 after deparaffinization and rehydration. Then, the peroxidase of the samples was quenched with 3% hydrogen peroxide. The samples were incubated with the as-mentioned primary antibodies overnight at 4°C. The samples were further incubated with the biotinylated anti-mouse secondary antibody IgG (1:1000; Abcam, cat. no. ab64255, RRID:AB_2757156) for 30 min at room temperature and avidin-biotin complex (ABC) reagent (Thermo Fisher Scientific). After washing the samples with PBS, the samples were incubated with 3,3′ Diaminobenzidine (DAB) reagent (Abcam) for 5 to 10 min. Last, the samples were stained with hematoxylin for 5 to 10 min

with washing and dehydrated by ethanol and xylene and then mounted by a coverslip for imaging.

qRT-PCR and RNA-seq

We performed quantitative reverse transcription polymerase chain reaction (qRT-PCR) according to our previous report (28). Briefly, TRIzol reagent (Invitrogen) was used to extract total RNA from the cell or tumor/organ samples according to the manufacturer's instructions. The concentration of the extracted RNA was quantified by NanoDrop One spectrophotometer (Nanorop Technologies), and the RNA was reverse transcribed into cDNA using RevertAid First Strand cDNA Synthesis Kit according to the manufacturer's instructions (Thermo Fisher Scientific). SYBR Green–based qRT-PCR was performed against GAPDH (glyceraldehyde-3-phosphate dehydrogenase; forward primer, 5′-AGGGCTGCTTT-TAACTCTGGTAAA-3′ and reverse primer, 5′-GAATTTGC-CATGGGTGGAAT-3′), human TRPV1 (forward primer, 5′-GGCTGTCTTCATCATCCTGCTGCT-3′ and reverse primer, 5′-GTTCTTGCTCTCCTGTGCGATCTTGT-3′), human TRPV2 (forward primer, 5′-CTTCCTTTTCGGCTTCGCTGTAG-3′ and reverse primer, 5′-GCACTGACTCTGTGGCATTGG-3′), human TRPV4 (forward primer, 5′-CTACGCTTCAGCCCTGGTCTC-3′ and reverse prime, 5′-GCAGTTGGTCTGGTCCTCATTG-3′), mouse TRPV4 (forward primer, 5′-TCACCGCCTACTATCAGC-CACT-3′ and reverse primer, 5′-GAACAGGACTCCTGTGAA-GAGC-3′), human TRPV6 (forward primer, 5′-GACCTCACAGAGATCGACTCCT-3′ and reverse primer, 5′-TACCGCTTCCACTTGAGGCTCA-3′), human Hsp70 (forward primer, 5′-CGGCAAGGTGGAGATCAT-3′ and reverse primer, 5′-GGTGTTCTGCGGGTTCAG-3′), mouse Hsp70 (forward primer, 5′-AGACTGTTGAGTTCTTTGTGTTTGGA-3′ and reverse primer, 5′-GAAGGACCCGACACAAGCAT-3′), human Sox2 (forward primer, 5′-GGGAAATGGGAGGGGTGCAAAA-GAGG-3′ and reverse primer, 5′-TTGCGTGAGTGTGGATGG-GATTGGTG-3′), human Nanog (forward primer, 5′-TCCAGGATTTTAACGTTCTGCT-3′ and reverse primer, 5′-TTCTTGCATCTGCTGGAGGC-3′), mouse Nanog (forward primer, 5′-CAGGAGTTTGAGGGTAGCTC-3′ and reverse primer, 5′-CGGTTCATCATGGTACAGTC-3′), and human Oct3/4 (forward primer, 5′-TATTCAGCCAAACGACCATCT-3′ and reverse primer, 5′- TCAGCTTCCTCCACCCACTT-3′). The above primers were purchased from Sangon Biotech (Shanghai). The gene expression levels were normalized to those of GAPDH as a housekeeping gene. All qRT-PCR results were performed from a sample size of $n = 4$.

The cDNA of each sample was sent to the company the Beijing Genomics Institute (BGI) Group to perform whole-transcriptome analysis. Briefly, the RNA [total RNA ≥ 200 ng; RNA integrity number (RIN) ≥ 200 ng; 28S/18S ≥ 1.0] from cells was harvested and then fragmented into 150–base pair paired-end pieces using the Bioruptor Pico system. The resulting fragments were then subjected to library preparation using BGI's standard protocol, which involved Proven DNBSEQ sequencing technology that combines the power of DNA nanoballs, PCR-free rolling circle replication, patterned nanoarrays, and combinatorial probe-anchor synthesis (cPAS) to deliver the resulting data. The samples met the criteria for further analysis, which included Q20 > 90% and Q30 > 85%. The hg19 RefSeq was used as the reference database for alignment using Tophat (v.2.0.12). The data were mapped to the hg19 reference database. DEG detection, gene ontology (GO) analysis of DEG, and other analyses based on gene expression were performed by BGI. GO terms with corrected P values (Q values) of 0.05 or less were considered significantly enriched among the DEGs on Dr. Tom's platform provided by BGI.

Western blotting assay

Cells were lysed by radioimmunoprecipitation assay lysis buffer (Beyotime), and the concentration of the extracted proteins was measured by the Bicinchoninic Acid Protein Assay Kit assay (Thermo Fisher Scientific). The equivalent amount of the protein of each sample was separated by 8 to 15% SDS–polyacrylamide gel electrophoresis (Beyotime); blocked with 5% fat-free milk powder (Aladdin) for 2 hours at room temperature; and incubated with primary antibodies to Hsp70, Hsp90 (Santa Cruz Biotechnology, cat. no. sc-101494, RRID:AB_1124018), HSF1, Oct3/4 (Santa Cruz Biotechnology, cat. no. sc-5279, RRID:AB_628051), Sox2 (Santa Cruz Biotechnology, cat. no. sc-365823, RRID:AB_10842165), STAT3, pSTAT3 (Santa Cruz Biotechnology, cat. no. sc-8059, RRID:AB_628292), PI3K (rabbit; Cell Signaling Technology, cat. no. 4292, RRID:AB_329869), pPI3K (rabbit; Cell Signaling Technology, cat. no. 4228, RRID:AB_659940), Akt (rabbit; Cell Signaling Technology, cat. no. 9272, RRID:AB_329827), pAkt (Tyr[326]; rabbit; Cell Signaling Technology, cat. no. 2968, RRID:AB_1264114), GADPH (all mouse, 1:1000; Santa Cruz Biotechnology), and Nanog (rat; 1:1000; Abcam). The primary antibodies were detected with goat anti-mouse or rat IgG-HRP (horseradish peroxidase; 1:2000; Santa Cruz Biotechnology). The blots were developed using Immobilon Western Chemiluminescent HRP Substrate (Merck) and were visualized and imaged by Gel Imaging System (Bio-Rad). To quantify the relative protein expression, all band intensities were normalized to GADPH or the respective control proteins. Three independent substrates were run for each blot and each group.

Image and statistical analysis

All schemes were drawn using Microsoft PowerPoint 365. ImageJ (NIH) was used for most electronic micrographs and cell images. Confocal images were analyzed by the Nikon confocal microscope in-built software. The colony size, nuclear size, and nuclear distribution profile were analyzed by ImageJ. The colony volume was measured via 3D reconstruction function of z-stack with volume measurement by the software NIS-Elements. The nuclear localization of a specific marker was measured by nuclear fluorescent/cytoplasmic fluorescent. For statistical analysis, analysis of variance (ANOVA) was performed on the statistics by using GraphPad Prism 8 or Microsoft Excel 365. All statistical sample sizes were described in the legends of the figures.

Supplementary Materials

This PDF file includes:
Figs. S1 to S30
Tables S1 to S3

View/request a protocol for this paper from *Bio-protocol*.

REFERENCES AND NOTES

1. X. Tang, T. B. Kuhlenschmidt, J. Zhou, P. Bell, F. Wang, M. S. Kuhlenschmidt, T. A. Saif, Mechanical force affects expression of an in vitro metastasis-like phenotype in HCT-8 cells. *Biophys. J.* **99**, 2460–2469 (2010).

2. V. Palmieri, D. Lucchetti, A. Maiorana, M. Papi, G. Maulucci, F. Calapà, G. Ciasca, R. Giordano, A. Sgambato, M. De Spirito, Mechanical and structural comparison between primary tumor and lymph node metastasis cells in colorectal cancer. *Soft Matter* **11**, 5719–5726 (2015).

3. G. Ciasca, M. Papi, E. Minelli, V. Palmieri, M. De Spirito, Changes in cellular mechanical properties during onset or progression of colorectal cancer. *World J. Gastroenterol.* **22**, 7203–7214 (2016).

4. T. Stylianopoulos, J. D. Martin, V. P. Chauhan, S. R. Jain, B. Diop-Frimpong, N. Bardeesy, B. L. Smith, C. R. Ferrone, F. J. Hornicek, Y. Boucher, L. L. Munn, R. K. Jain, Causes, consequences, and remedies for growth-induced solid stress in murine and human tumors. *Proc. Natl. Acad. Sci. U.S.A.* **109**, 15101–15108 (2012).

5. R. S. Stowers, A. Shcherbina, J. Israeli, J. J. Gruber, J. Chang, S. Nam, A. Rabiee, M. N. Teruel, M. P. Snyder, A. Kundaje, O. Chaudhuri, Matrix stiffness induces a tumorigenic phenotype in mammary epithelium through changes in chromatin accessibility. *Nat. Biomed. Eng.* **3**, 1009–1019 (2019).

6. K. M. Wisdom, K. Adebowale, J. Chang, J. Y. Lee, S. Nam, R. Desai, N. S. Rossen, M. Rafat, R. B. West, L. Hodgson, O. Chaudhuri, Matrix mechanical plasticity regulates cancer cell migration through confining microenvironments. *Nat. Commun.* **9**, 4144 (2018).

7. K. R. Levental, H. Yu, L. Kass, J. N. Lakins, M. Egeblad, J. T. Erler, S. F. T. Fong, K. Csiszar, A. Giaccia, W. Weninger, M. Yamauchi, D. L. Gasser, V. M. Weaver, Matrix crosslinking forces tumor progression by enhancing integrin signaling. *Cell* **139**, 891–906 (2009).

8. E. Brauchle, J. Kasper, R. Daum, N. Schierbaum, C. Falch, A. Kirschniak, T. E. Schäffer, K. Schenke-Layland, Biomechanical and biomolecular characterization of extracellular matrix structures in human colon carcinomas. *Matrix Biol.* **68-69**, 180–193 (2018).

9. J. M. Northcott, I. S. Dean, J. K. Mouw, V. M. Weaver, Feeling stress: The mechanics of cancer progression and aggression. *Front. Cell Dev. Biol.* **6**, 17 (2018).

10. H. T. Nia, M. Datta, G. Seano, P. Huang, L. L. Munn, R. K. Jain, Quantifying solid stress and elastic energy from excised or in situ tumors. *Nat. Protoc.* **13**, 1091–1105 (2018).

11. Q. Xu, G. Schett, C. Li, Y. Hu, G. Wick, Mechanical stress-induced heat shock protein 70 expression in vascular smooth muscle cells is regulated by Rac and Ras small G proteins but not mitogen-activated protein kinases. *Circ. Res.* **86**, 1122–1128 (2000).

12. M. Akerfelt, R. I. Morimoto, L. Sistonen, Heat shock factors: Integrators of cell stress, development and lifespan. *Nat. Rev. Mol. Cell Biol.* **11**, 545–555 (2010).

13. N. , A. W. Truman, Cracking the chaperone code: Cellular roles for Hsp70 phosphorylation. *Trends Biochem. Sci.* **42**, 932–935 (2017).

14. W. H. Chooi, B. P. Chan, Compression loading-induced stress responses in intervertebral disc cells encapsulated in 3D collagen constructs. *Sci. Rep.* **6**, 26449 (2016).

15. D. Weng, J. H. Penzner, B. Song, S. Koido, S. K. Calderwood, J. Gong, Metastasis is an early event in mouse mammary carcinomas and is associated with cells bearing stem cell markers. *Breast Cancer Res.* **14**, R18 (2012).

16. Y. Li, E. Kumacheva, Hydrogel microenvironments for cancer spheroid growth and drug screening. *Sci. Adv.* **4**, eaas8998 (2018).

17. J. R. Choi, K. W. Yong, J. Y. Choi, A. C. Cowie, Recent advances in photo-crosslinkable hydrogels for biomedical applications. *Biotechniques* **66**, 40–53 (2019).

18. S. H. D. Wong, W. K. R. Wong, C. H. N. Lai, J. Oh, Z. Li, X. Chen, W. Yuan, L. Bian, Soft polymeric matrix as a macroscopic cage for magnetically modulating reversible nanoscale ligand presentation. *Nano Lett.* **20**, 3207–3216 (2020).

19. V. Hintze, M. Schnabelrauch, S. Rother, Chemical modification of hyaluronan and their biomedical applications. *Front. Chem.* **10**, 830671 (2022).

20. L. Bian, C. Hou, E. Tous, R. Rai, R. L. Mauck, J. A. Burdick, The influence of hyaluronic acid hydrogel crosslinking density and macromolecular diffusivity on human MSC chondrogenesis and hypertrophy. *Biomaterials* **34**, 413–421 (2013).

21. X. Chen, N. C.-H. Lai, K. Wei, R. Li, M. Cui, B. Yang, S. H. D. Wong, Y. Deng, J. Li, X. Shuai, L. Bian, Biomimetic presentation of cryptic ligands via single-chain nanogels for synergistic regulation of stem cells. *ACS Nano* **14**, 4027–4035 (2020).

22. M. Jang, J. An, S. W. Oh, J. Y. Lim, J. Kim, J. K. Choi, J.-H. Cheong, P. Kim, Matrix stiffness epigenetically regulates the oncogenic activation of the Yes-associated protein in gastric cancer. *Nat. Biomed. Eng.* **5**, 114–123 (2021).

23. C. Liu, H. Pei, F. Tan, Matrix stiffness and colorectal cancer. *Onco. Targets. Ther.* **13**, 2747–2755 (2020).

24. M. Lekka, A tip for diagnosing cancer. *Nat. Nanotechnol.* **7**, 691–692 (2012).

25. I. Acerbi, L. Cassereau, I. Dean, Q. Shi, A. Au, C. Park, Y. Y. Chen, J. Liphardt, E. S. Hwang, V. M. Weaver, Human breast cancer invasion and aggression correlates with ECM stiffening and immune cell infiltration. *Integr. Biol.* **7**, 1120–1134 (2015).

26. M. Cavo, M. Fato, L. Peñuela, F. Beltrame, R. Raiteri, S. Scaglione, Microenvironment complexity and matrix stiffness regulate breast cancer cell activity in a 3D in vitro model. *Sci. Rep.* **6**, 35367 (2016).

27. S. Nam, V. K. Gupta, H.-P. Lee, J. Y. Lee, K. M. Wisdom, S. Varma, E. M. Flaum, C. Davis, R. B. West, O. Chaudhuri, Cell cycle progression in confining microenvironments is

28. regulated by a growth-responsive TRPV4-PI3K/Akt-p27^Kip1 signaling axis. *Sci. Adv.* **5**, eaaw6171 (2019).

28. S. H. D. Wong, X. Xu, X. Chen, Y. Xin, L. Xu, C. H. N. Lai, J. Oh, W. K. R. Wong, X. Wang, S. Han, W. You, X. Shuai, N. Wong, Y. Tan, L. Duan, L. Bian, Manipulation of the nanoscale presentation of integrin ligand produces cancer cells with enhanced stemness and robust tumorigenicity. *Nano Lett.* **21**, 3225–3236 (2021).

29. M. E. Dolega, M. Delarue, F. Ingremeau, J. Prost, A. Delon, G. Cappello, Cell-like pressure sensors reveal increase of mechanical stress towards the core of multicellular spheroids under compression. *Nat. Commun.* **8**, 14056 (2017).

30. H. T. Nia, H. Liu, G. Seano, M. Datta, D. Jones, N. Rahbari, J. Incio, V. P. Chauhan, K. Jung, J. D. Martin, V. Askoxylakis, T. P. Padera, D. Fukumura, Y. Boucher, F. J. Hornicek, A. J. Grodzinsky, J. W. Baish, L. L. Munn, R. K. Jain, Solid stress and elastic energy as measures of tumour mechanopathology. *Nat. Biomed. Eng.* **1**, 0004 (2017).

31. W. Lee, N. Kalashnikov, S. Mok, R. Halaoui, E. Kuzmin, A. J. Putnam, S. Takayama, M. Park, L. McCaffrey, R. Zhao, R. L. Leask, C. Moraes, Dispersible hydrogel force sensors reveal patterns of solid mechanical stress in multicellular spheroid cultures. *Nat. Commun.* **10**, 144 (2019).

32. C. Yang, M. W. Tibbitt, L. Basta, K. S. Anseth, Mechanical memory and dosing influence stem cell fate. *Nat. Mater.* **13**, 645–652 (2014).

33. Y. L. Han, A. F. Pegoraro, H. Li, K. Li, Y. Yuan, G. Xu, Z. Gu, J. Sun, Y. Hao, S. K. Gupta, Y. Li, W. Tang, H. Kang, L. Teng, J. J. Fredberg, M. Guo, Cell swelling, softening and invasion in a three-dimensional breast cancer model. *Nat. Phys.* **16**, 101–108 (2020).

34. M. E. Feder, G. E. Hofmann, Heat-shock proteins, molecular chaperones, and the stress response: Evolutionary and ecological physiology. *Annu. Rev. Physiol.* **61**, 243–282 (1999).

35. Q. Xu, Role of heat shock proteins in atherosclerosis. *Arterioscler. Thromb. Vasc. Biol.* **22**, 1547–1559 (2002).

36. H. Yang, Y. Yao, H. Li, L. W. C. Ho, B. Yin, W.-Y. Yung, K. C.-F. Leung, A. F.-T. Mak, C. H. J. Choi, Promoting intracellular delivery of sub-25 nm nanoparticles via defined levels of compression. *Nanoscale* **10**, 15090–15102 (2018).

37. B. Metzler, R. Abia, M. Ahmad, F. Wernig, O. Pachinger, Y. Hu, Q. Xu, Activation of heat shock transcription factor 1 in atherosclerosis. *Am. J. Pathol.* **162**, 1669–1676 (2003).

38. F. Frezzato, V. Raggi, F. Martini, V. Severin, V. Trimarco, A. Visentin, E. Scomazzon, B. Accordi, S. Bresolin, F. Piazza, M. Facco, G. Basso, G. Semenzato, L. Trentin, HSP70/HSF1 axis, regulated via a PI3K/AKT pathway, is a druggable target in chronic lymphocytic leukemia. *Int. J. Cancer* **145**, 3089–3100 (2019).

39. M. Chatterjee, M. Andrulis, T. Stühmer, E. Müller, C. Hofmann, T. Steinbrunn, T. Heimberger, H. Schraud, S. Kressmann, H. Einsele, R. C. Bargou, The PI3K/Akt signaling pathway regulates the expression of Hsp70, which critically contributes to Hsp90-chaperone function and tumor cell survival in multiple myeloma. *Haematologica* **98**, 1132–1141 (2013).

40. M. Di-Luoffo, Z. Ben-Meriem, P. Lefebvre, M. Delarue, J. Guillermet-Guibert, PI3K functions as a hub in mechanotransduction. *Trends Biochem. Sci.* **46**, 878–888 (2021).

41. A. P. Koivisto, M. G. Belvisi, R. Gaudet, A. Szallasi, Advances in TRP channel drug discovery: From target validation to clinical studies. *Nat. Rev. Drug Discov.* **21**, 41–59 (2022).

42. C. F. L. Fernandes, R. P. Iglesia, M. I. Melo-Escobar, M. B. Prado, M. H. Lopes, Chaperones and beyond as key players in pluripotency maintenance. *Front. Cell Dev. Biol.* **7**, 150 (2019).

43. Y. S. Son, J. H. Park, Y. K. Kang, J.-S. Park, H. S. Choi, J. Y. Lim, J. E. Lee, J. B. Lee, M. S. Ko, Y.-S. Kim, J.-H. Ko, H. S. Yoon, K.-W. Lee, R. H. Seong, S. Y. Moon, C. J. Ryu, H. J. Hong, Heat shock 70-kDa protein 8 isoform 1 is expressed on the surface of human embryonic stem cells and downregulated upon differentiation. *Stem Cells* **23**, 1502–1513 (2005).

44. M. M. Setati, E. Prinsloo, V. M. Longshaw, P. A. Murray, D. H. Edgar, G. L. Blatch, Leukemia inhibitory factor promotes Hsp90 association with STAT3 in mouse embryonic stem cells. *IUBMB Life* **62**, 61–66 (2010).

45. F. Okumura, A. J. Okumura, M. Matsumoto, K. I. Nakayama, S. Hatakeyama, TRIM8 regulates Nanog via Hsp90β-mediated nuclear translocation of STAT3 in embryonic stem cells. *Biochim. Biophys. Acta* **1813**, 1784–1792 (2011).

46. Y. Teng, L. Ngoka, Y. Mei, L. Lesoon, J. K. Cowell, HSP90 and HSP70 proteins are essential for stabilization and activation of WASF3 metastasis-promoting protein. *J. Biol. Chem.* **287**, 10051–10059 (2012).

47. M. Pitrone, G. Pizzolanti, L. Tomasello, A. Coppola, L. Morini, G. Pantuso, R. Ficarella, V. Guarnotta, F. Perrini, F. Giorgino, C. Giordano, NANOG plays a hierarchical role in the transcription network regulating the pluripotency and plasticity of adipose tissue-derived stem cells. *Int. J. Mol. Sci.* **18**, 1107 (2017).

48. J. D. Lathia, H. Liu, Overview of cancer stem cells and stemness for community oncologists. *Target. Oncol.* **12**, 387–399 (2017).

49. W. Xie, Z. Du, Y. Chen, N. Liu, Z. Zhong, Y. Shen, L. Tang, Identification of metastasis-associated genes in triple-negative breast cancer using weighted gene co-expression network analysis. *Evol. Bioinform. Online* **16**, 1176934320954868 (2020).

50. R. Mitra, C. M. Adams, W. Jiang, E. Greenawalt, C. M. Eischen, Pan-cancer analysis reveals cooperativity of both strands of microRNA that regulate tumorigenesis and patient survival. *Nat. Commun.* **11**, 968 (2020).

51. L. Xie, Y. Liao, L. Shen, F. Hu, S. Yu, Y. Zhou, Y. Zhang, Y. Yang, D. Li, M. Ren, Z. Yuan, Z. Yang, Identification of the miRNA-mRNA regulatory network of small cell osteosarcoma based on RNA-seq. *Oncotarget* **8**, 42525–42536 (2017).

52. J. J. Zhou, X.-G. Deng, X.-Y. He, Y. Zhou, M. Yu, W.-C. Gao, B. Zeng, Q.-B. Zhou, Z.-H. Li, R.-F. Chen, Knockdown of NANOG enhances chemosensitivity of liver cancer cells to doxorubicin by reducing MDR1 expression. *Int. J. Oncol.* **44**, 2034–2040 (2014).

53. A. Saito, M. Tojo, Y. Kumagai, H. Ohzawa, H. Yamaguchi, H. Miyato, A. Sadatomo, D. Naoi, G. Ota, K. Koinuma, H. Horie, A. K. Lefor, N. Sata, J. Kitayama, Flow cytometry detection of cell type-specific expression of programmed death receptor ligand-1 (PD-L1) in colorectal cancer specimens. *Heliyon* **7**, e05880 (2021).

54. S. Khetan, M. Guvendiren, W. R. Legant, D. M. Cohen, C. S. Chen, J. A. Burdick, Degradation-mediated cellular traction directs stem cell fate in covalently crosslinked three-dimensional hydrogels. *Nat. Mater.* **12**, 458–465 (2013).

55. P. Kasioumi, P. Vrazeli, P. Vezyraki, S. Zerikiotis, C. Katsouras, A. Damalas, C. Angelidis, Hsp70 (HSP70A1A) downregulation enhances the metastatic ability of cancer cells. *Int. J. Oncol.* **54**, 821–832 (2019).

Science Advances

Mechanical manipulation of cancer cell tumorigenicity via heat shock protein signaling

Siu Hong Dexter Wong, Bohan Yin, Zhuo Li, Weihao Yuan, Qin Zhang, Xian Xie, Youhua Tan, Nathalie Wong, Kunyu Zhang, and Liming Bian

View the article online
https://www.science.org/doi/10.1126/sciadv.adg9593
Permissions
https://www.science.org/help/reprints-and-permissions

Use of this article is subject to the Terms of service